



Structural displacement estimation by fusing vision camera and accelerometer using hybrid computer vision algorithm and adaptive multi-rate Kalman filter



Zhanxiong Ma ^a, Jaemook Choi ^a, Peipei Liu ^{a,b}, Hoon Sohn ^{a,b,*}

^a Department of Civil and Environmental Engineering, Korea Advanced Institute of Science and Technology, Daejeon, South Korea

^b Center for 3D Printing Nondestructive Testing, Korea Advanced Institute of Science and Technology, Daejeon, Republic of Korea

ARTICLE INFO

Keywords:

Displacement estimation
Accelerometer
Data fusion
Vision camera
Feature-matching algorithm
Phase-based optical flow algorithm
Adaptive multi-rate Kalman filter

ABSTRACT

Structural displacement monitoring is essential because displacement can provide critical information regarding the health condition of civil structures. However, the precise estimation of structural displacement remains a challenge. This paper describes a displacement estimation technique that fuses asynchronous acceleration and vision measurements at different sampling rates. A hybrid computer vision (CV) algorithm and an adaptive multi-rate Kalman filter are integrated to efficiently estimate high-sampling displacement from low-sampling vision measurement and high-sampling acceleration measurement. An initial calibration algorithm is proposed to automatically determine active pixels and two scale factors required in the hybrid CV algorithm without any prior knowledge or ad-hoc thresholding. The proposed technique was experimentally validated and high-sampling displacements were accurately estimated in real-time with less than 1.5 mm error, indicating the potential of the proposed technique for practical applications in long-term continuous structural displacement monitoring.

1. Introduction

Structural displacement sensing is vital for civil structures because displacement helps understand the structure's global behavior and evaluate its safety [1]. Displacement is adopted as a safety indicator in structural design codes of several countries [2–4]. For example, the USA design code requires the displacement of a bridge to be less than 1/1000 of its length under normal vehicle and pedestrian loads [2]. In addition, displacement is useful in evaluating the bridge load-carrying capacity [5,6], identifying modal parameters of structures [7,8], and updating the finite element model of structures [9].

Several techniques have been developed to directly measure or indirectly estimate structural displacement, and they can be categorized into (1) contact and (2) non-contact techniques. Linear variable differential transformers (LVDT) [10] and accelerometers [6] are typical contact-type sensors. However, installing an LVDT on the field is not convenient, and low-frequency displacement cannot be accurately estimated using an accelerometer. The real-time kinematic global navigation satellite system (RTK-GNSS) [11], laser Doppler vibrometer (LDV) [12], and radar systems [13,14] are typical non-contact sensors.

However, RTK-GNSS has a low sampling rate of 20 Hz and limited accuracy of approximately 7–10 mm. Although LDV and radar systems can measure high-accuracy and high-sampling displacement, these devices are expensive and require a rigid ground for installation, making them impractical in civil infrastructure applications. A vision camera is another option for non-contact structural displacement monitoring. The movement of a target structure is tracked by a vision camera installed on rigid ground using various computer vision (CV) algorithms [15–21], such as template matching [15,16], feature-matching (FM) [17,18], and optical flow algorithms [19,20]. However, the target movement initially estimated from vision measurements is in a pixel unit, and a scale factor is required to obtain the target displacement in physical length units. The scale factor is commonly estimated from the target physical size, but it is cumbersome to measure the target physical size on the field. Moreover, these CV algorithms fail to estimate the displacement in real time at a high sampling rate, owing to the high computational cost.

To address the aforementioned limitations, researchers have attempted to fuse vision cameras and accelerometers for structural displacement estimation. Vision-based displacement estimated at a low sampling rate and acceleration measured at a high sampling rate were

* Corresponding author at: Department of Civil and Environmental Engineering, Korea Advanced Institute of Science and Technology, Daejeon, South Korea.
E-mail address: hoonsohn@kaist.ac.kr (H. Sohn).

combined to estimate the displacement with a high sampling rate. However, this process still requires a target physical size for scale factor estimation [22,23]. The authors previously proposed a real-time structural displacement estimation technique by fusing asynchronous vision and acceleration measurements [24]. The scale factor was first estimated automatically using acceleration measurements. Next, the low-sampling vision-based displacement estimated using an improved FM (IFM) algorithm was fused with the acceleration measurement by an adaptive multi-rate Kalman filter (AMKF) developed for real-time high-sampling displacement estimation. However, the low-sampling displacement estimated with the IFM algorithm suffers from low-accuracy issues, particularly for subtle pixel translation, thereby deteriorating the estimation accuracy of the final high-sampling displacement.

Recently, a phase-based optical flow (POF) algorithm was developed to estimate displacement from vision measurements [25], and several studies have demonstrated that the algorithm is highly sensitive to the subtle movement of a target [26–30]. In brief, this algorithm extracts the local phase from vision measurements and estimates the target displacement using the phase variation. However, the conversion of the phase variation to displacement requires spatial differential and matrix inverse operations [26], which may not guarantee a stable displacement estimation when vision measurement has a high noise level and poor resolution. Furthermore, although the POF algorithm has been widely adopted, most studies have focused on the frequency components of the estimated displacement for damage detection [27,28] and modal identification [29,30]; therefore, less attention has been paid to the amplitude accuracy of the estimated displacement. In addition, the selection of active pixels within a region of interest (ROI), that is, the pixels whose phases are related to the target movement, requires an ad-hoc threshold [30]. Moreover, phase-wrapping may occur with a large target movement [31], resulting in inaccurate displacement estimation.

Motivated by the aforementioned (1) low-accuracy issue of our previous technique using vision camera and accelerometer [24] and (2) potential of the existing POF algorithm in improving displacement estimation accuracy and its drawbacks, this study proposes a high-accuracy displacement estimation technique by integrating the existing POF algorithm to our previous technique and addressing the drawbacks of the existing POF algorithm. A hybrid CV algorithm, that is, the combined POF and FM algorithm, was first proposed to accurately estimate displacement from low-sampling vision measurements. This algorithm requires active pixels and two scale factors (converting phase and translation to displacements, respectively), which are automatically determined by the proposed initial calibration algorithm. Thereafter, an AMKF is adopted to fuse the vision-based displacement estimated at a low sampling rate with the acceleration measured at a high sampling rate, and the final displacement is estimated in real time with a high sampling rate and improved accuracy. The main contributions of this study are as follows: (1) a hybrid CV algorithm is proposed by combining the FM and POF algorithms to estimate a high-accuracy displacement from vision measurement even in the presence of large structural displacement; (2) two scale factors for converting phase and translation to displacement, respectively, are automatically estimated without any prior knowledge; (3) active pixels within an ROI are automatically selected without any ad-hoc threshold; and (4) the displacement estimation accuracy is significantly improved compared to previous techniques in both laboratory and field tests.

The remainder of this paper is organized as follows. The POF algorithm for displacement estimation is briefly reviewed in [Section 2](#), followed by an explanation of the proposed technique in [Section 3](#). The performance of the proposed technique is first validated by indoor single-story building test and outdoor shaking-table test in [Section 4](#). In [Section 5](#), a field test is conducted on a steel box-girder pedestrian bridge to further validate the proposed technique. The concluding remarks are presented in [Section 6](#).

2. Review of the POF algorithm for vision-based displacement estimation

To obtain a vision-based displacement estimation, a vision camera placed on rigid ground is aimed at a natural or artificial target on a structure. The displacement is then estimated by tracking the target movement within the vision measurements, that is, a series of vision images. It has been demonstrated that a local phase extracted from vision images is highly sensitive to subtle target movement [25] and is adopted for structural displacement estimation, that is, the POF algorithm [26]. The procedure for estimating the target vertical displacement at the i^{th} time step using the POF algorithm is briefly illustrated below ([Fig. 1](#)). Note that the field of view (FOV) of the camera is usually rather large, and only a portion of an image, including the target (i.e., ROI), is cropped and processed for structural displacement estimation.

Assuming that the i^{th} ROI with a size of $M \times N$ and an intensity of $I_i(x, y)$ at a spatial location (x, y) is obtained, its local phase $\varphi_i(x, y)$ and amplitude $A_i(x, y)$ are extracted in the vertical direction by calculating the spatial convolution between the ROI and a complex Gabor filter ($G_2^v + jH_2^v$),

$$A_i(x, y)e^{i\varphi_i(x, y)} = (G_2^v + jH_2^v) \otimes I_i(x, y) \quad (1)$$

Next, the full-field vertical displacement at the i^{th} time step is estimated from the phase variation compared with the initial phase extracted from the 1st ROI ($\varphi_1(x, y)$):

$$u_i(x, y) = -\alpha \left[\frac{\partial \varphi_i(x, y)}{\partial x} \right]^{-1} [\varphi_i(x, y) - \varphi_1(x, y)] = -\alpha \left[\frac{\partial \varphi_i(x, y)}{\partial x} \right]^{-1} \varphi_{1,i}(x, y) \quad (2)$$

where α denotes a scale factor for converting a pixel unit to a length unit, and $\varphi_{1,i}(x, y)$ is the phase variation between the 1st and i^{th} ROIs. Finally, the target displacement is estimated as the spatial average of $u_i(x, y)$,

$$u_i = \frac{1}{M \times N} \sum_{(x,y) \in \text{ROI}} u_i(x, y) = \frac{\alpha}{M \times N} \sum_{(x,y) \in \text{ROI}} \left\{ - \left[\frac{\partial \varphi_i(x, y)}{\partial x} \right]^{-1} \varphi_{1,i}(x, y) \right\} \quad (3)$$

More details regarding the POF algorithm can be found in the study by Chen et al. [26].

However, this study has several limitations. First, $-\left[\frac{\partial \varphi_i(x, y)}{\partial x} \right]^{-1}$ in Eq. (3) acts as a scale factor for converting phase variation into translation in a pixel unit, but the spatial differential and matrix inverse operation may not guarantee a stable scale factor, thereby leading to an inaccurate displacement estimation. Note that, several studies have simplified Eq. (3) to:

$$u_i = \frac{\beta}{M \times N} \sum_{(x,y) \in \text{ROI}} \varphi_{1,i}(x, y) = \beta \bar{\varphi}_{1,i} \quad (4)$$

and directly adopted the spatial average of the phase variation ($\bar{\varphi}_{1,i}$) for model identification or damage detection without calculating β [28]. Here, β denotes a scale factor for converting phase to displacement. Second, not all pixels within the ROI are active, and it is highly probable that incorrect pixels are selected as active pixels with an improper threshold [32]. Third, the application of the algorithm is limited to small target movements to avoid the phase-wrapping issue [31,33].

3. Development of the proposed structural displacement estimation technique

This study proposes a displacement estimation technique that uses a collocated vision camera and accelerometer measurements. A vision camera and accelerometer were placed at the same location on a structure where the displacement was to be estimated ([Fig. 2\(a\)](#)). Assuming that the structure vibrates in a horizontal direction (X

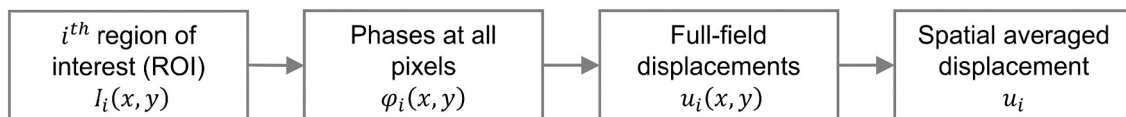


Fig. 1. Overview of the conventional POF algorithm for displacement estimation.

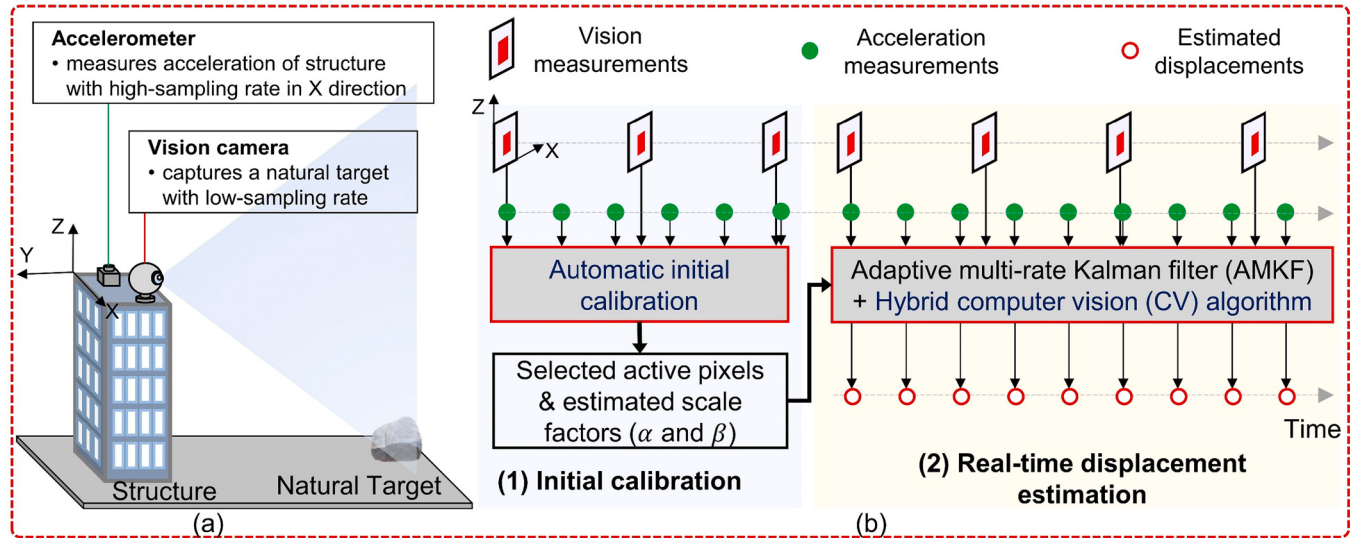


Fig. 2. Overview of the proposed displacement estimation technique: (a) sensor setup and (b) overall flowchart.

direction), the accelerometer measured the acceleration of the structure with a high sampling rate in the same direction and the vision camera tracked a fixed target from the surroundings of the structure with a low sampling rate. Note that, it is assumed that the structure has only in-plane vibration, and the axes of the image plane and real-world plane are aligned. An AMKF and a hybrid CV algorithm were used to fuse vision and acceleration measurements for estimating displacement in real time with high accuracy and a high sampling rate. Considering that the hybrid CV algorithm requires active pixels and two scale factors, short-period vision and acceleration measurements were used for active pixel selection and scale factor estimation. Therefore, as shown in Fig. 2 (b), the proposed technique was divided into two parts: (1) automatic initial calibration for active pixel selection and scale factor estimation (Section 3.1) and (2) real-time displacement estimation using an AMKF and a hybrid CV algorithm (Section 3.2).

3.1. Automatic initial calibration for active pixel selection and scale factor estimation

To estimate a high-accuracy displacement from vision measurement, even in the presence of a large structural displacement, this study proposes a hybrid CV algorithm by combining FM and POF algorithms. Note that Eq. (4) was adopted in this study instead of Eq. (3). Therefore, the proposed hybrid CV algorithm requires scale factors (α and β) to be

estimated and active pixels to be selected. In this section, we propose an automatic initial calibration algorithm to estimate the scale factors (α and β) and select the active pixels. Assuming that vision and acceleration measurements are recorded for a short period (e.g., 50 s in this study), the initial calibration algorithm is explained step-by-step as follows:

Step 1: Large motion removal by updating ROI location

First, ROIs were cropped from the recorded short-period vision measurement with a fixed ROI location (denoted as the original ROIs), and a translation (d) was estimated from the original ROIs using an FM algorithm [34]. Then, the updated ROIs were obtained by updating the ROI location at each time step using d (Fig. 3). Considering that the ROI location is discrete at pixel resolution, the shift in the ROI location (d_{ROI}) can be expressed as follows:

$$d_{ROI} = \text{round}(d) \quad (5)$$

The primary purpose of this step is to remove large motions in the original ROIs to ensure that the residual motion in the updated ROIs is sufficiently small to avoid the phase-wrapping issue in the POF algorithm.

Step 2: Estimation of scale factor (α)

First, the displacement (u_a) was estimated from the recorded short-period acceleration measurements using double integration. Then, a band-pass filter was applied to u_a and d to obtain the filtered displacement (u_a^f) and filtered translation (d^f), respectively. The lower cut-off

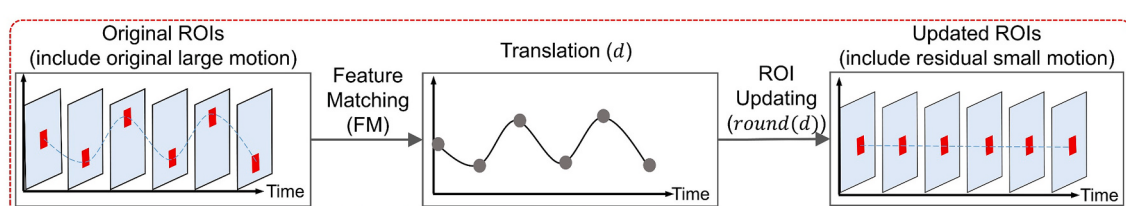


Fig. 3. ROI location updating using the translation estimated by a FM algorithm to remove large motion.

frequency of the filter was set to be sufficiently high to remove the low-frequency drift in u_a , and the upper cut-off frequency was set to 1/10 of the vision camera's sampling rate [24]. Finally, the scale factor (α) for converting translation to displacement was estimated as the ratio between u_a^f and d^f using the least squares estimation (LSE) algorithm (Fig. 4). Here, u_a^f was downsampled to match the sampling rate of d^f before applying the LSE algorithm [24].

Step 3: Selection of active pixels and estimation of scale factor (β)

- (a) The residual displacement (u_r) in the updated ROIs was estimated as follows:

$$u_r = u_a - ad_{ROI} = u_a - \alpha \text{ round}(d) \quad (6)$$

and a filtered residual displacement (u_r^f) was estimated by band-pass filtering u_r with the same cutoff frequencies as in Step 2 (Fig. 5(a)).

- (b) The full-field phase ($\varphi(x,y)$) was first extracted from the updated ROIs using the POF algorithm and then band-pass filtered to obtain a filtered phase ($\varphi^f(x,y)$). Subsequently, a correlation coefficient ($\rho(x,y)$) was calculated between u_r^f and $\varphi^f(x,y)$ for each pixel. Here, u_r^f was downsampled to match the sampling rate of $\varphi^f(x,y)$ before calculating the correlation coefficient (Fig. 5(b)).
- (c) A threshold (ρ_t) was initially set to $\min\{|\rho(x,y)|\}$, and pixels with an absolute value of the correlation coefficient above the threshold were initially selected as active pixels. An averaged phase ($\bar{\varphi}^f$) was obtained as the spatial average of the filtered phases of all the active pixels. Next, the scale factor (β) for the converting phase to displacement was estimated as the ratio between u_r^f and $\bar{\varphi}^f$ using the LSE algorithm. The determination coefficient (R^2) was calculated to evaluate the accuracy of the estimation (Fig. 5(c)).
- (d) As ρ_t value changed from $\min\{|\rho(x,y)|\}$ to $\max\{|\rho(x,y)|\}$, the corresponding β and R^2 values were obtained. The optimized threshold ($\hat{\rho}_t$) was determined with the maximum value of R^2 , and was used to finalize the active pixels and estimate the final scale factor (β) (Fig. 5(d)).

3.2. Real-time displacement estimation using an AMKF and a hybrid CV algorithm

After selecting active pixels and estimating scale factors (α and β), the displacement is estimated in real time from asynchronous vision and acceleration measurements using an AMKF and the proposed hybrid CV algorithm. Note that, although other multi-rate Kalman filters are available for fusing measurements from different sensors, they all require synchronous measurements of the sensors [35–38]. Therefore, the AMKF previously developed by the authors for asynchronous vision and acceleration measurements [24] was used in this study for displacement estimation.

3.2.1. AMKF-based fusion of asynchronous vision and acceleration measurement

Based on the availability of acceleration and vision measurements,

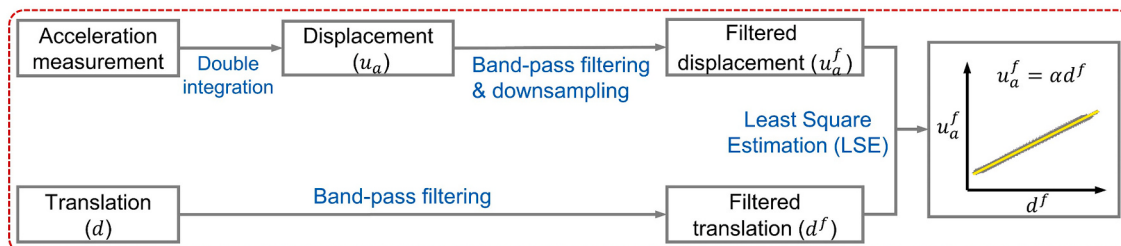


Fig. 4. Flowchart of estimating scale factor (α) for converting translation to displacement.

three different types of time steps were defined, and the AMKF was formulated accordingly, as shown in Fig. 6. In a Type-I time step, the vision measurement was not available, and a state (\hat{x}_k) was estimated using the state and acceleration at the previous time step (\hat{x}_{k-1} and a_{k-1} , respectively):

$$\hat{x}_k = A(\Delta t_a) \hat{x}_{k-1} + B(\Delta t_a) a_{k-1}; A(\Delta t_a) = \begin{bmatrix} 1 & \Delta t_a \\ 0 & 1 \end{bmatrix}; B(\Delta t_a) = \begin{bmatrix} \Delta t_a^2/2 \\ \Delta t_a \end{bmatrix} \quad (7)$$

and its covariance (\hat{P}_k) was obtained as follows:

$$\hat{P}_k = A(\Delta t_a) \hat{P}_{k-1} A^T(\Delta t_a) + q B(\Delta t_a) B^T(\Delta t_a) \quad (8)$$

Here, \hat{x}_k includes two entities, corresponding to the displacement and velocity estimated at $t = k\Delta t_a$, respectively. Δt_a and q denote the time interval and noise variance, respectively, of the acceleration measurements. The q value can be easily estimated using laboratory testing.

In a Type-II time step, a prior state and its covariance (\hat{y}_i^- and \hat{G}_i^- , respectively) were first estimated as:

$$\hat{y}_i^- = A(\Delta t_1) \hat{x}_k + B(\Delta t_1) a_k \quad (9)$$

$\hat{G}_i^- = A(\Delta t_{i,k}) \hat{P}_k A^T(\Delta t_{i,k}) + q B(\Delta t_{i,k}) B^T(\Delta t_{i,k}); \Delta t_{i,k} = i\Delta t_d - k\Delta t_a$, where i denotes the i^{th} time step of the vision measurements and Δt_d denotes the time interval of the vision measurements. Using \hat{y}_i^- and \hat{G}_i^- , a hybrid CV algorithm was proposed and applied to estimate displacement u_i from vision measurements. Details are provided in Section 3.2.2. Thereafter, the noise variance of u_i (R_i) was estimated adaptively as [39]

$$R_i = \gamma R_{i-1} + (1 - \gamma)(\eta_i^2 - \hat{H}\hat{G}_i^- H^T), 0 < \gamma < 1 \quad (10)$$

$\eta_i = u_i - \hat{H}\hat{y}_i^-$, $H = [1 \ 0]^T$ where γ denotes the forgetting factor. Subsequently, the filter gain (K) was calculated as follows:

$$K = \hat{P}_i H^T (H \hat{P}_i H^T + R_i)^{-1} \quad (11)$$

The final state and its covariance (\hat{y}_i^+ and \hat{G}_i^+ , respectively) were updated as follows:

$$\hat{y}_i^+ = (I - KH)\hat{y}_i^- + Ku_i \quad (12)$$

$$\hat{G}_i^+ = (I - KH)\hat{G}_i^-$$

In Type-III time step, a state was estimated as follows, and state covariance was estimated accordingly. Details of the AMKF can be found in the study by Ma et al. [24].

$$\hat{x}_{k+1} = A(\Delta t_{k+1,i}) \hat{y}_i^+ + B(\Delta t_{k+1,i}) a_k \quad (13)$$

$$\Delta t_{k+1,i} = (k+1)\Delta t_a - i\Delta t_d$$

3.2.2. Hybrid CV algorithm for high-accuracy displacement estimation

A hybrid CV algorithm was proposed in this study to estimate the displacement from vision measurements for both subtle and large structural displacements, as shown in Fig. 7. First, the movement of the

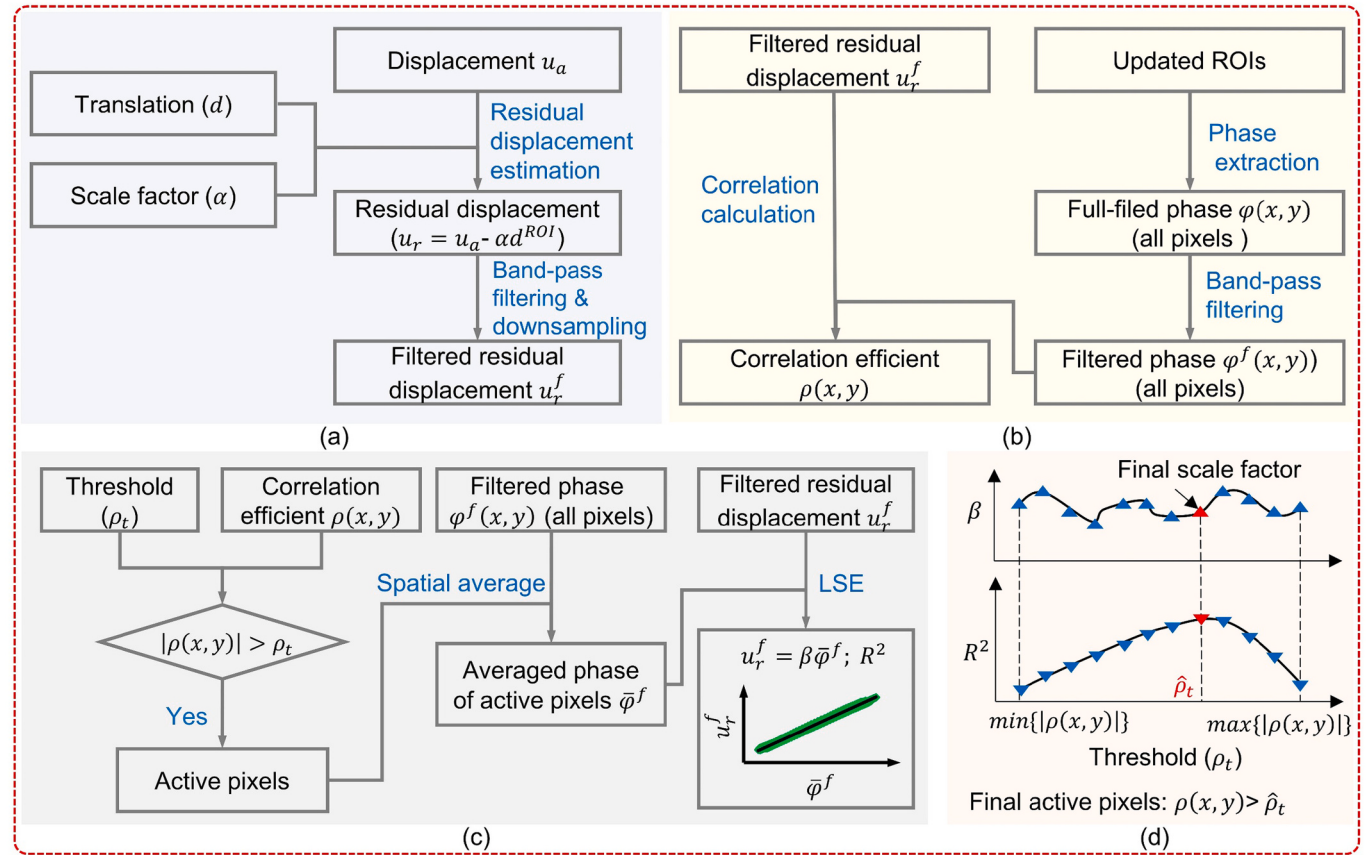


Fig. 5. Flowchart of selecting active pixels and estimating scale factor (β) for converting phase to displacement: (a) estimation of the filtered residual displacement, (b) calculation of the correlation efficient for all pixels, (c) selection of active pixels with an initial threshold ($\rho_t = \min\{|\rho(x, y)|\}$), and (d) optimization of the threshold (ρ_t) by maximizing R^2 value for final active pixel selection and β estimation.

ROI location (d_i^{ROI}) was predicted, and the ROI at the i^{th} frame was updated accordingly.

$$d_i^{ROI} = \text{round}\left(\frac{\widehat{y}_i(1)}{\alpha}\right) \quad (14)$$

where $\widehat{y}_i(1)$, that is, the first entity of \widehat{y}_i , denotes the predicted displacement. Then, the residual displacement between the 1st and i^{th} ROIs is given as follows:

$$u_i^r = \widehat{y}_i(1) - w_i - \alpha d_i^{ROI} \quad (15)$$

where w_i denotes the estimation error in $\widehat{y}_i(1)$ and its variance is $\widehat{G}_i(1, 1)$, that is, the first entity of \widehat{G}_i . Assuming that w_i follows a normal distribution, a 99.7% confidence interval of u_i^r can be estimated as

$$|u_i^r| \leq u_{i,\max}^r = 3\sqrt{\widehat{G}_i(1, 1)} + 0.5\alpha \quad (16)$$

If $u_{i,\max}^r < \beta\pi$, the phase variation between the 1st and i^{th} ROIs is smaller than π , and the POF algorithm can be directly applied to extract the averaged phase variation ($\bar{\varphi}_{1,i}$) from the active pixels. Finally, the vision-based displacement (u_i) can be estimated as:

$$u_i = \alpha d_i^{ROI} + \beta \bar{\varphi}_{1,i} = \alpha \text{round}\left(\frac{\widehat{y}_i(1)}{\alpha}\right) + \beta \bar{\varphi}_{1,i} \quad (17)$$

If $u_{i,\max}^r \geq \beta\pi$, the phase variation of the 1st and i^{th} ROIs is equal to or larger than π , and the POF algorithm cannot be directly applied because of the phase-wrapping issue. Thus, a translation (d_i) between the 1st and i^{th} ROIs was first estimated using an FM algorithm with automatic mismatch rejections [24]. Subsequently, d_i was used to update the i^{th}

ROI again, and the POF algorithm was applied to the 2nd updated i^{th} ROI to extract the phase variation ($\bar{\varphi}_{1,i}$). Considering that the total movement of the ROI location in this case becomes,

$$d_i^{ROI} = \text{round}\left(\frac{\widehat{y}_i(1)}{\alpha} + d_i\right) \quad (18)$$

vision-based displacement (u_i) can be finally estimated as follows:

$$u_i = \alpha d_i^{ROI} + \beta \bar{\varphi}_{1,i} = \alpha \text{round}\left(\frac{\widehat{y}_i(1)}{\alpha} + d_i\right) + \beta \bar{\varphi}_{1,i} \quad (19)$$

4. Laboratory validation

4.1. Indoor single-story building model test

The proposed technique was first validated using a single-story building model, as shown in Fig. 8. The building model was rigidly connected to an ELECTRO-SEIS APS-400 shaking table, which provided horizontal movement for the model (Fig. 8(a)). A force-balance-type uniaxial accelerometer and a vision camera were installed on top of the building model (Fig. 8(b)). The ground-truth displacement of the model was measured using a Polytec PSV-400-M4 LDV [40] (Fig. 8(c)). The vision measurement originally recorded at 29.97 Hz was down-sampled to 10 ($\approx 29.97/3$) Hz, while analog measurements from the accelerometer and LDV were discrete at a sampling rate of 100 Hz using a National Instruments USB-6343 data acquisition device. Furthermore, the vision and acceleration measurements were aligned on the same time axis using a correlation-based algorithm [22]. Fig. 8(e) shows the camera FOV and initial ROI. The distance between the target included in

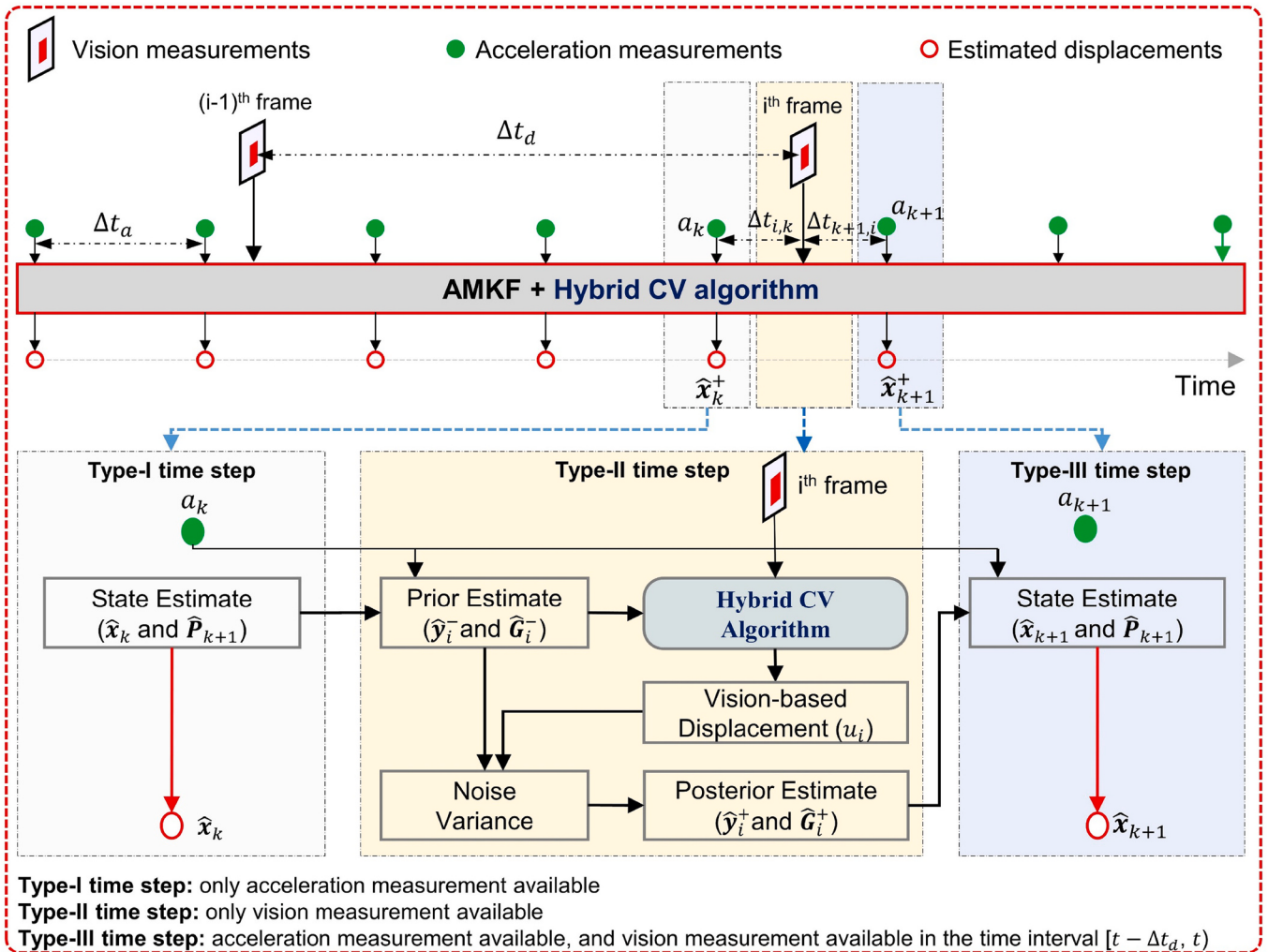


Fig. 6. Overview of the fusion of asynchronous vision and acceleration measurement using the AMKF for structural displacement estimation.

the ROI and camera was approximately 3 m (Fig. 8(d)). Three different signals were input into the shaking table: (1) a 1 Hz sinusoidal signal, (2) a chirp signal with frequency varying from DC to 3 Hz, and (3) a vibration signal recorded from a real bridge.

First, vision and acceleration measurements under 1 Hz sinusoidal signal excitation were used for automatic initial calibration. Fig. 9 compares the estimation results of scale factor (β) with and without large motion in vision measurement (i.e., Step 1 in Section 3.1) and demonstrates the necessity of removing large motion for β estimation. In the presence of large motion, no linear relationship was observed between the filtered phase and filtered displacement from the acceleration measurement owing to the serious phase-wrapping issue (Fig. 9(a)). However, a linear relationship was clearly observed after the large motion was removed, and β was estimated to be -3.8093 mm/rad with R^2 equal to 0.9821 (Fig. 9(b)). Here, scale factor (α) was estimated as 2.11 mm/pixel.

Next, the performance of the proposed technique was compared with that of an existing technique [24]. The existing technique used an IMF algorithm to estimate the displacement from vision measurement, which was further fused with the acceleration measurement for the final displacement estimation. The vision-based displacements estimated using the proposed and existing techniques are compared in Fig. 10. The noise levels of the estimated vision-based displacements were evidently reduced by using the proposed hybrid CV algorithm, resulting in a maximum 53% RMSE reduction. Table 1 lists the final estimated

displacements obtained using both the techniques [24] after fusing vision-based displacement and acceleration measurements. The proposed technique reduced the RMSEs of the estimated displacements by approximately 42% compared with the existing technique. Note that the existing POF algorithm [26] could not estimate the displacement correctly in this test owing to the serious phase-wrapping issue, and the corresponding estimation results were omitted.

4.2. Outdoor shaking table test

The proposed technique was validated using an outdoor shaking table test, as shown in Fig. 11. The accelerometer and vision camera used in the previous test were installed on a steel plate (Fig. 11(a)). The shaking table, which was rigidly connected to the plate, moved the plate vertically. A window of a surrounding building at a distance of approximately 63 m was selected as the fixed target (Fig. 11(b)), and the camera FOV and initial ROI, which included the selected target, are shown in Fig. 11(c). Other experimental parameters were identical to those used in the previous indoor single-story building model test unless stated otherwise.

First, vision and acceleration measurements under a sinusoidal signal excitation of 1 Hz were used for automatic initial calibration. Next, displacements were estimated using both the existing [24] and proposed techniques under three different excitations, and the RMSEs of the estimated displacements are summarized in Table 2. The proposed

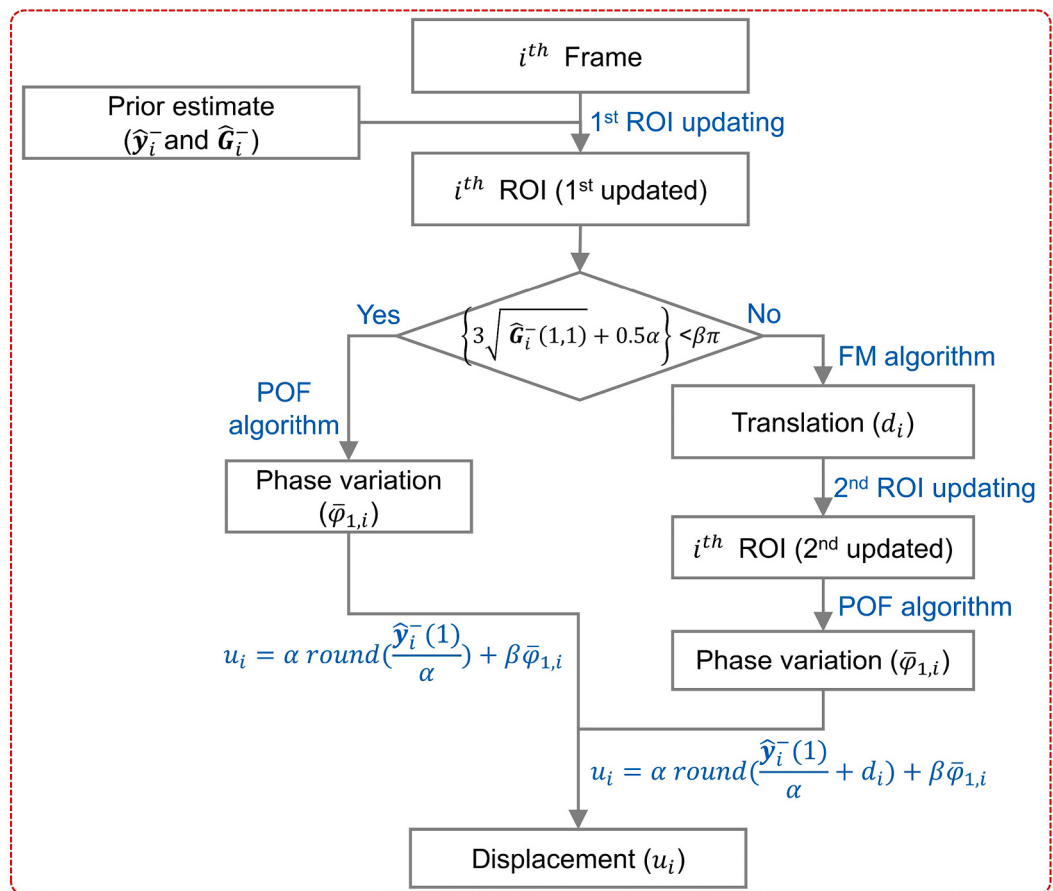


Fig. 7. Flowchart of the proposed hybrid CV algorithm for displacement estimation from vision measurement.

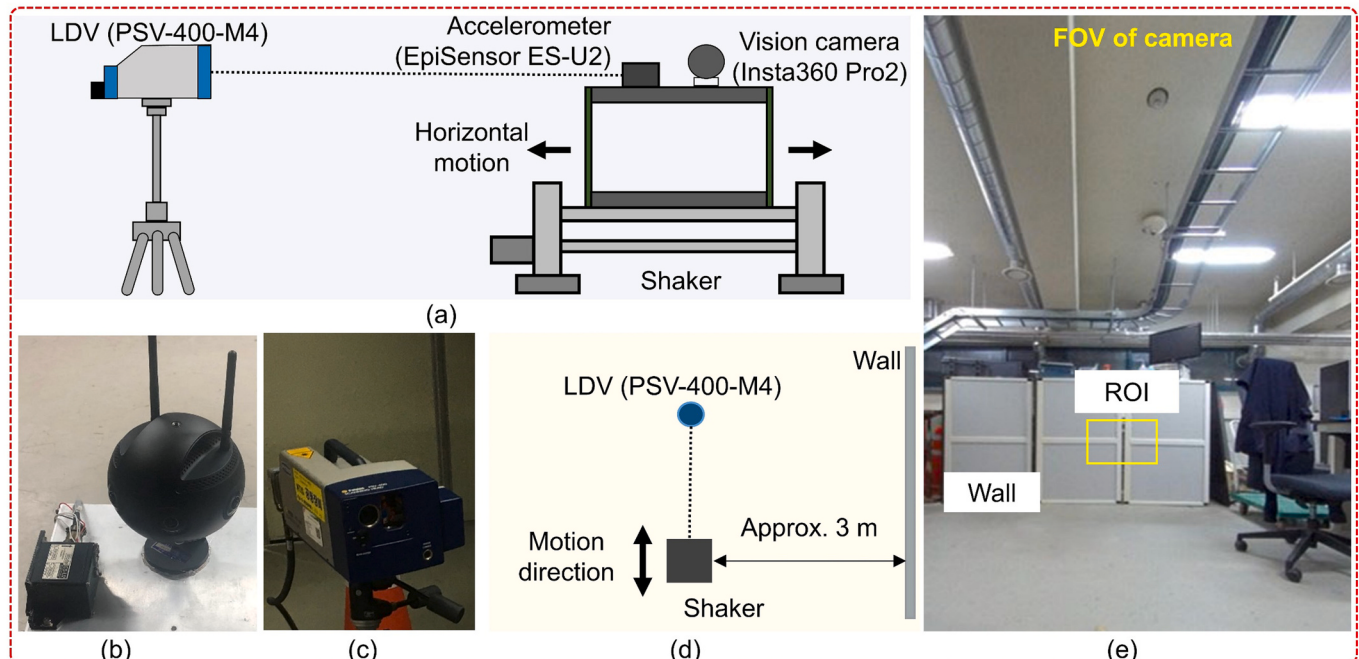


Fig. 8. Configuration of indoor single-story building model test: (a) overview, (b) force-balance-type uniaxial accelerometer and a vision camera installed on the top of the building model, (c) LDV used for reference displacement measurement, (d) 3-m distance between the shaker and the wall, and (e) camera FOV and the initial ROI.

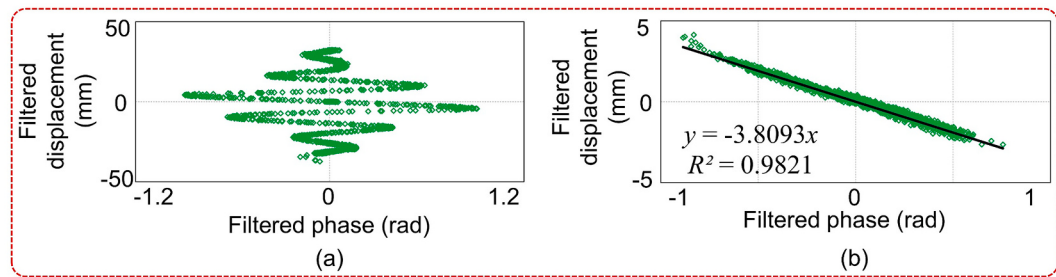


Fig. 9. Estimation results of the scale factor (β): (a) without and (b) with large motion.

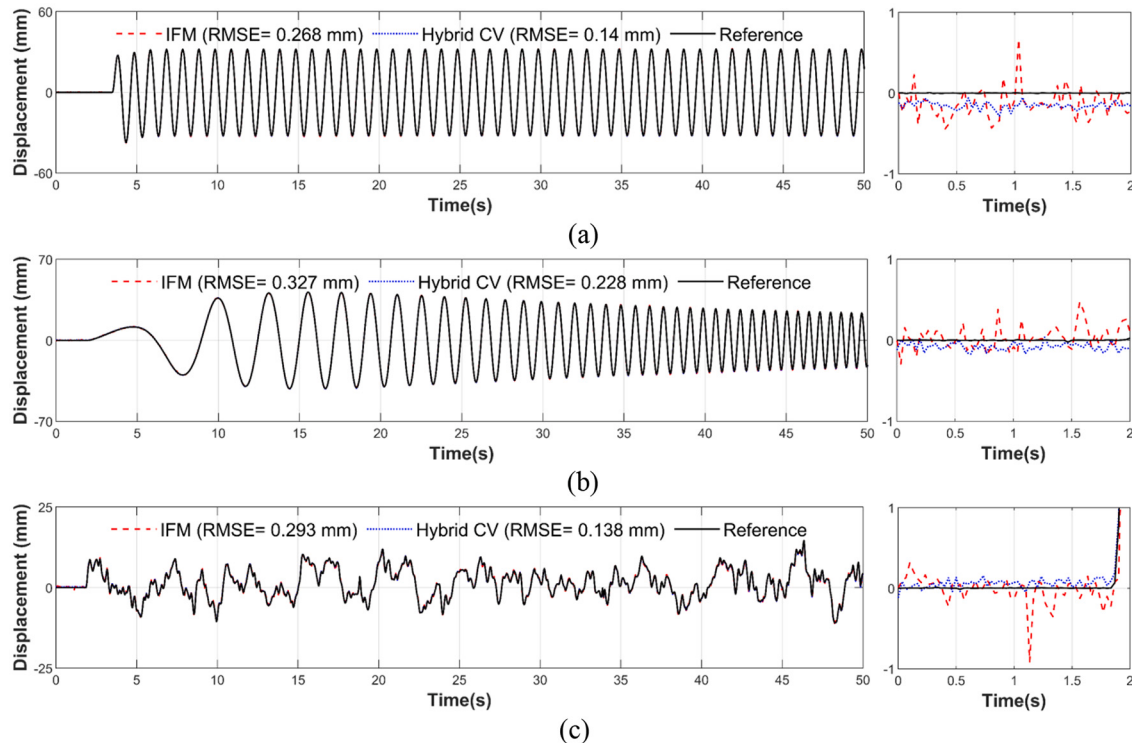


Fig. 10. Comparison of vision-based displacements estimated using the existing IFM [24] and proposed hybrid CV algorithms in the indoor single-story building model test: (a) 1 Hz sinusoidal signal, (b) chirp signal, and (c) recorded real bridge vibration excitation.

Table 1

Comparison of RMSEs of final displacements estimated using the existing and proposed techniques after fusing vision-based displacements and acceleration measurements [24] in the indoor single-story building model test.

Excitations	Existing technique [24] (AMKF + IMF algorithm)	Proposed technique (AMKF + Hybrid CV algorithm)	RMSE reduction
1 Hz sinusoidal	0.237 mm	0.129 mm	45.57%
Chirp	0.262 mm	0.200 mm	23.66%
Recorded real bridge vibration	0.291 mm	0.130 mm	55.33%
Average	0.263 mm	0.153 mm	41.90%

technique reduced the RMSEs by 51% compared to the existing technique and estimated the displacement accurately with less than 1.5 mm error.

In addition, the performance of the proposed technique was compared with that of an existing POF algorithm [26]. Note that the existing POF algorithm used only vision measurements; therefore, only vision-based displacements estimated by the POF algorithm and the

proposed hybrid CV algorithm were compared. Because the vision camera was far from the target, only subtle pixel movement existed in the vision measurements, and phase-wrapping did not occur in this test. Thus, the main differences between the proposed hybrid CV and the existing POF algorithms are as follows: (1) active pixel selection and (2) scale factor estimation (Table 3).

Fig. 12 shows the initial ROI and active pixels selected by the proposed and existing algorithms. For the existing algorithm, the threshold of active pixel selection was 1/5 of the mean of the 30 pixels with the largest amplitudes within the ROI. The vision-based displacements estimated by both the algorithms are compared in Fig. 13. The proposed hybrid CV algorithm was able to accurately estimate the displacement from vision measurements with an error of less than 2 mm. However, large errors are observed in vision-based displacements estimated using the existing POF algorithm, which are mainly attributed to inaccurate scale factor estimation.

Next, the active pixel selection effectiveness of the proposed initial calibration algorithm was validated. Active pixels were selected in three different ways: (1) all pixels within the ROI, (2) pixels with a local amplitude above a threshold [26], and (3) pixels selected by the proposed algorithm. The corresponding scale factors (β) were estimated

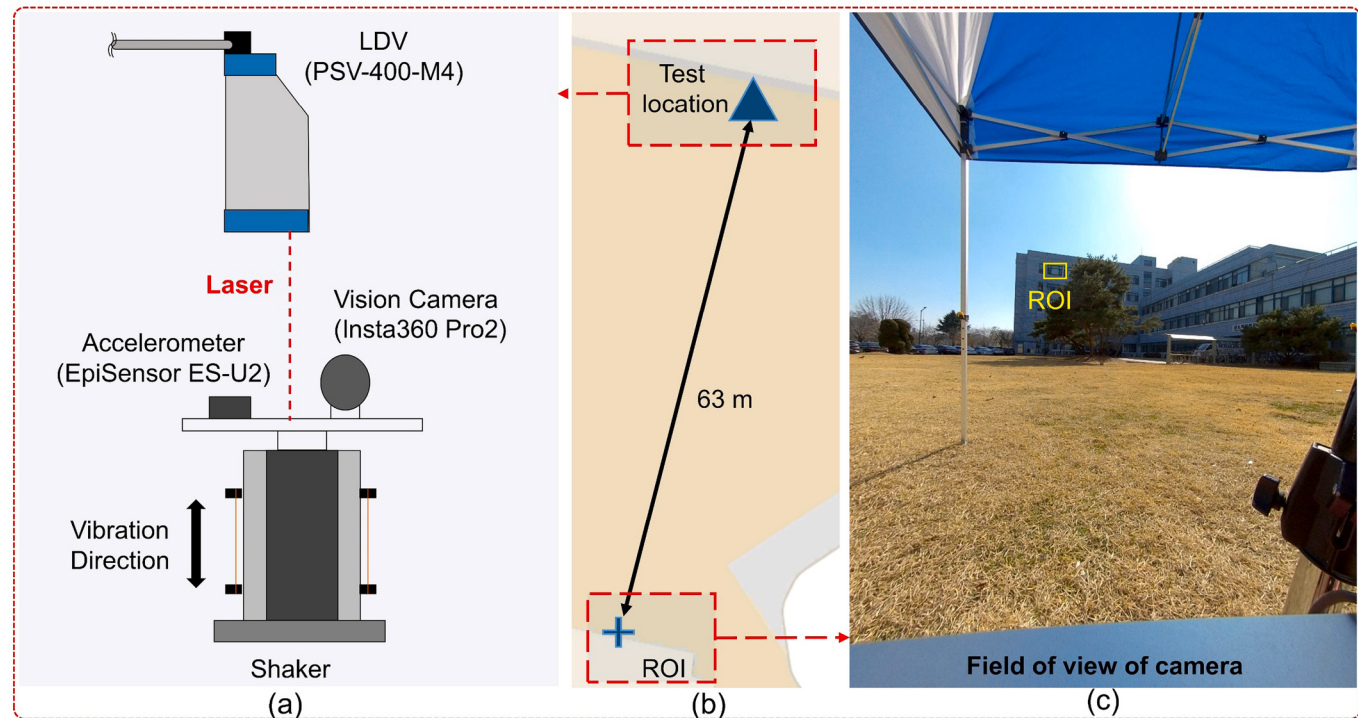


Fig. 11. Configuration of the outdoor shaking table test: (a) sensor setup, (b) 63-m distance between the vision camera and the target, and (c) FOV of the vision camera and the initial ROI.

Table 2

Comparison of RMSEs of the final displacements estimated using the existing [24] and proposed techniques in outdoor shaking table test.

Excitations	Existing technique [24] (AMKF + IMF algorithm)	Proposed technique (AMKF + Hybrid CV algorithm)	RMSE reduction
1 Hz sinusoidal	2.66 mm	1.28 mm	51.88%
Chirp	3.18 mm	1.42 mm	55.35%
Recorded real bridge vibration	2.29 mm	1.25 mm	45.41%
Average	2.71 mm	1.32 mm	51.29%

Table 3

Comparison between the existing POF and proposed hybrid CV algorithms.

	Active pixel selection	Scale factor estimation
Existing POF algorithm [26]	Pixels with the local amplitude above 1/5 of the mean of the 30 pixels with largest amplitudes within the ROI	Eq. (3)
Proposed hybrid CV algorithm	Automatic initial calibration	Eq. (4) with automatic initial calibration

using the proposed algorithm. As shown in Fig. 14, active pixels selected using the proposed initial calibration algorithm presented the largest R^2 value. Displacements were then estimated from vision measurements using different active pixels and their corresponding β . The best performance was achieved using the active pixels selected by the proposed algorithm under all three excitations, as listed in Table 4.

The computation costs of the proposed technique have been analyzed on a desktop PC configured with Intel i7-6700 CPU (3.4 GHz) and 8 GB RAM. Though the time required for the image acquisition and processing varied slightly at different time steps, the averaged time was less than 0.1 s, allowing real-time vision-based displacement estimation

at 10 Hz. Then, by fusing the vision-based displacement at 10 Hz with the acceleration measurement at 100 Hz, the final displacement was estimated at 100 Hz in real-time.

5. Field test on a pedestrian steel box-girder bridge

The proposed technique was validated on a pedestrian steel box-girder bridge located in Daejeon, Korea, and experimental configuration is shown in Fig. 15. The displacement was estimated at 1/4 span point of the bridge, and the same vision camera and accelerometer (Fig. 15(c)) were placed at the displacement estimation location. A Polytec RSV-150 LDV (Fig. 15(d)) was installed on the ground to measure the reference displacement with less than 1 μm resolution [41], which was used to evaluate the displacement estimation performance of the proposed technique. Fig. 15(e) shows the FOV of the camera. A traffic signal structure at a distance of approximately 2 m was available in the FOV, and the ROI was initially cropped to cover the structure joint. Three different excitations were considered: (1) Case 1: four people jumping at 1/4 span point, (2) Case 2: two people jumping at 1/4 span point and sixteen people slowly passing the bridge; and (3) Case 3: sixteen people slowly passing the bridge.

Initial calibration was performed using measurements of the camera and the accelerometer when four people jumped at 1/4 span point (Case 1). Two scale factors (α and β) were estimated as -1.233 mm/rad and 1.359 mm/pixel , respectively. The displacements estimated using the proposed technique under all three excitations were compared with those estimated using the existing technique [24] (Fig. 16). Although the displacement of the bridge was relatively small, up to a few millimeters, the proposed algorithm could estimate the displacement accurately with an error of less than 0.06 mm. Compared to existing techniques, the proposed technique reduces the RMSE by approximately 63%.

Next, a performance comparison with the existing POF algorithm [26] and the effectiveness validation of the active pixel selection were performed, as in the case of the outdoor shaking table test, and the results are summarized in Tables 5 and 6, respectively. Large errors were

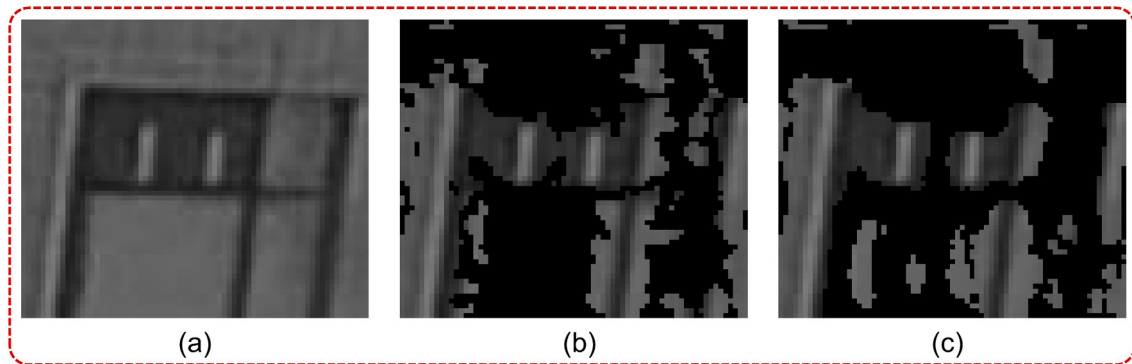


Fig. 12. (a) Initial ROI in the outdoor shaking table test, and the corresponding active pixels selected by (b) existing POF algorithm [26] and (c) proposed hybrid CV algorithm.

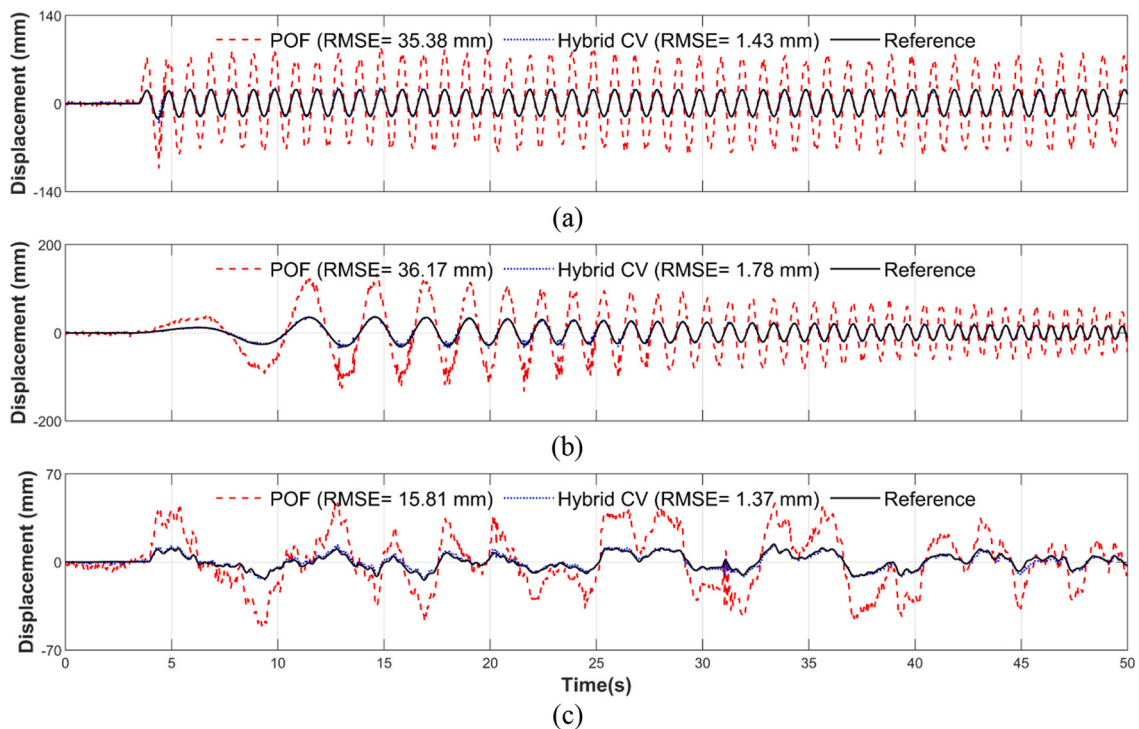


Fig. 13. Comparison of vision-based displacement estimated using the existing POF algorithm [26], and proposed hybrid CV algorithm in the outdoor shaking table test: (a) 1 Hz sinusoidal, (b) chirp, and (c) recorded real bridge vibration excitation.

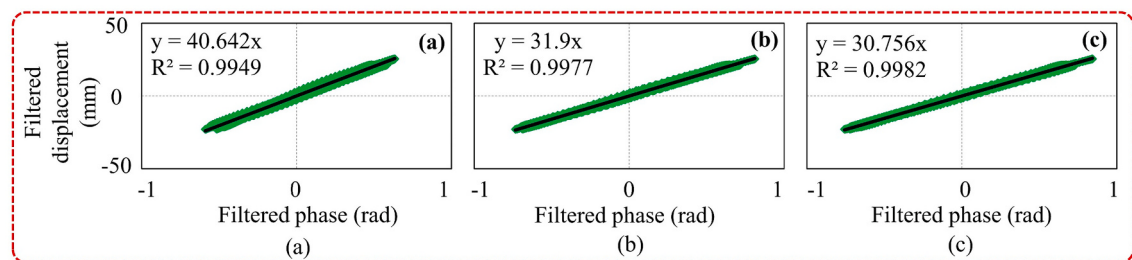


Fig. 14. Comparison of scale factors (β) estimated using (a) all pixels with ROI, (b) pixels with the local amplitude above a threshold [26], (c) active pixels selected by the proposed initial calibration algorithm.

again observed in the displacements estimated using the existing POF algorithm owing to the inaccurate scale factor estimation (Table 5). The active pixels selected by the proposed algorithm achieved the best

displacement estimation performance under all three excitations, as shown in Table 6.

Finally, displacement estimation performance of the proposed

Table 4

Comparison of RMSEs of the displacements estimated with different active pixels in outdoor shaking table test (Unit: mm).

Excitations	All pixels within ROI	pixels with the local amplitude above a threshold [26]	pixels selected by the proposed initial calibration algorithm
1 Hz sinusoidal	1.84	1.62	1.43
Chirp	2.38	1.88	1.78
Recorded real bridge vibration	1.69	1.37	1.37
Average	1.97	1.62	1.53

hybrid CV algorithm were compared with the existing FM algorithm [18], and the results are summarized in Table 7. Because the displacements of the bridge were only a few millimeters, subtle pixel translations of the target were produced in vision measurements. Considering that the proposed hybrid CV algorithm is more sensitive to subtle pixel translations of the target compared to the existing FM algorithm, it reduced the RMSEs of the estimated displacements by approximately 74%.

6. Conclusions

This paper describes a displacement estimation technique that fuses asynchronous acceleration and vision measurements at different sampling rates. The primary contributions of this study lie in the automatic initial calibration for active pixel selection and scale factor estimation, and development of a hybrid computer vision (CV) algorithm by combining phase-based optical flow and feature-matching algorithms. The feasibility of the proposed technique was experimentally validated through indoor single-story building, outdoor shaking table, and

pedestrian bridge tests. The following conclusions were drawn from this study:

- (1) The hybrid CV algorithm significantly reduced the noise level of the displacement estimated from vision measurement compared to the feature matching algorithm. In addition, unlike the conventional phase-based optical flow algorithm, the hybrid CV algorithm successfully estimated displacement from vision measurement even in the presence of large structural displacement.
- (2) The proposed initial calibration algorithm selected active pixels without any ad-hoc thresholding, and displacements estimated using the selected active pixels were better than those estimated using the active pixels selected by the existing threshold-based algorithm [26]. In addition, the scale factor estimated by the initial calibration algorithm resulted in approximately 78% RMSE reduction in displacement estimation compared to the scale factor estimated by the existing algorithm [26].
- (3) The errors of the final estimated displacements were reduced by approximately 50% in indoor single-story building, outdoor shaking table, and pedestrian bridge tests compared to the existing technique [24]. The overall RMSEs were 0.153 mm, 1.32 mm and 0.043 mm for these three tests, respectively.

Although the proposed technique shows a potential for practical applications in long-term continuous structural displacement monitoring, there are still limitations that need to be addressed. Firstly, the proposed technique estimates only in-plane displacement. However, large-scale civil structures often exhibit displacements in all six degrees-of-freedom. In addition, the presented tests estimated displacement only for a short time period without explicitly considering environmental

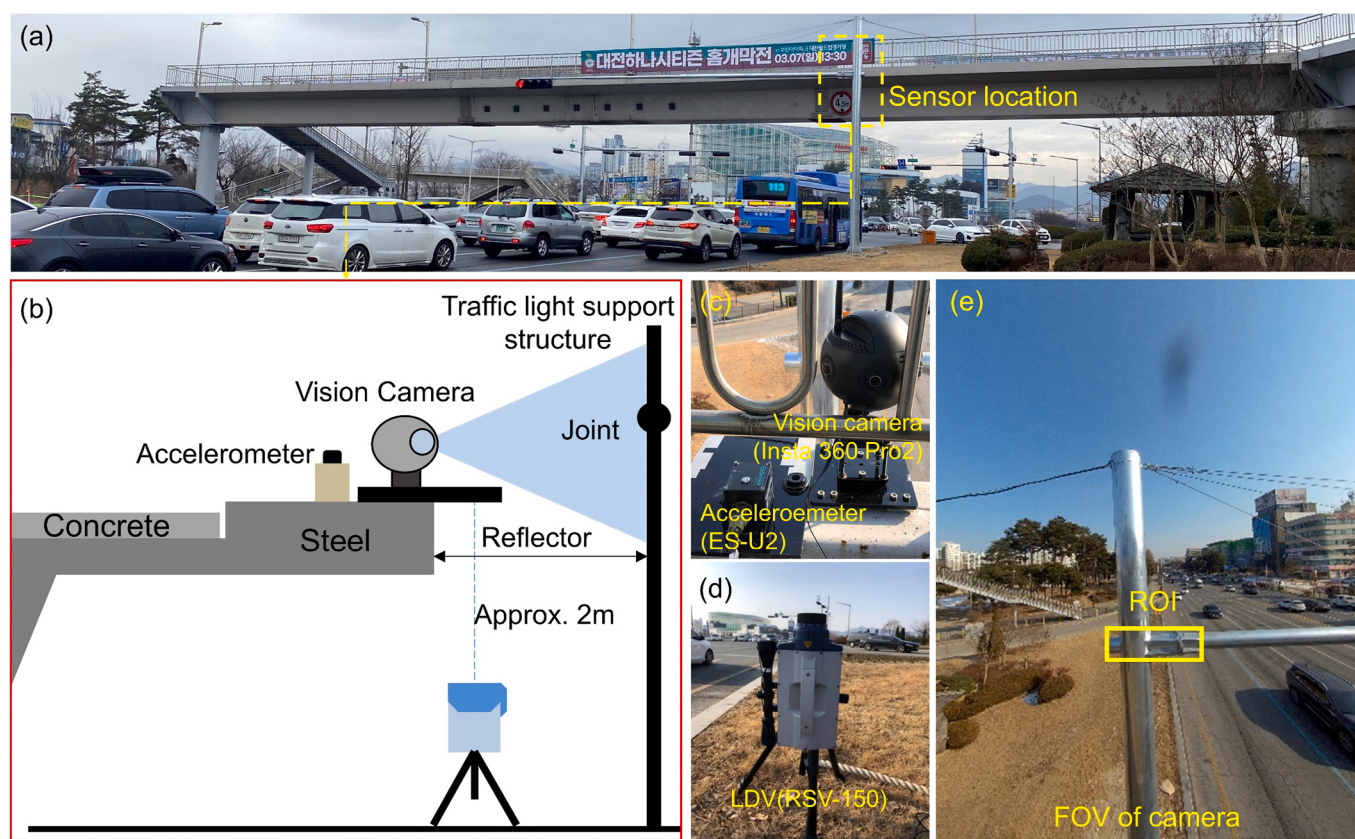


Fig. 15. Configuration of pedestrian steel box-girder bridge test: (a) overview of the bridge, (b) sensor setup, (c) an accelerometer and a vision camera used for displacement estimation, (d) an LDV for reference displacement measurement, and (e) FOV of camera and the initial ROI.

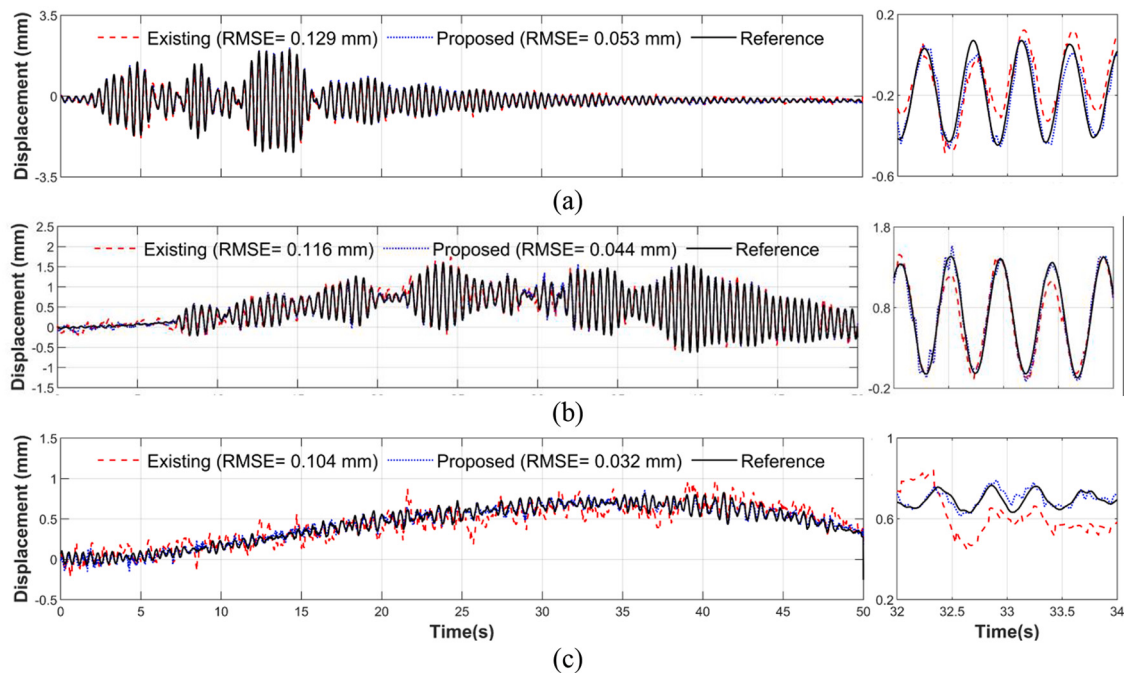


Fig. 16. Comparison of pedestrian bridge displacements estimated by the existing [24] and proposed techniques [24]: (a) case 1, (b) case 2, and (c) case 3.

Table 5

Comparison of RMSEs of vision-based displacement estimated using the existing POF algorithm and proposed hybrid CV algorithm in pedestrian steel box-girder bridge test.

Excitations	The existing POF algorithm [26]	The proposed hybrid CV algorithm	RMSE reduction
Case 1	0.268 mm	0.059 mm	77.99%
Case 2	0.229 mm	0.048 mm	79.04%
Case 3	0.130 mm	0.032 mm	75.38%
Average	0.209 mm	0.046 mm	77.83%

Table 6

Comparison of RMSEs of vision-based displacements estimated with different active pixels in pedestrian steel box-girder bridge test.

Excitations	All pixels within ROI	pixels with the local amplitude above a threshold [26]	pixels selected by the proposed initial calibration algorithm
Case 1	0.069 mm	0.062 mm	0.059 mm
Case 2	0.062 mm	0.054 mm	0.048 mm
Case 3	0.051 mm	0.035 mm	0.032 mm
Average	0.061 mm	0.050 mm	0.046 mm

Table 7

Comparison of RMSEs of vision-based displacement estimated using the existing FM algorithm and proposed hybrid CV algorithm in pedestrian steel box-girder bridge test.

Excitations	The existing FM algorithm [18]	The proposed hybrid CV algorithm	RMSE reduction
Case 1	0.160 mm	0.059 mm	63.12%
Case 2	0.163 mm	0.048 mm	70.55%
Case 3	0.189 mm	0.032 mm	83.07%
Average	0.171 mm	0.046 mm	73.1%

variations such as illumination and temperature. Future work is warranted to address these limitations, and to make the proposed technique more attractive for long-term continuous monitoring of real structural

displacements.

Declaration of Competing Interest

The authors declare that they have no known competing financial interests or personal relationships that could have appeared to influence the work reported in this paper.

Acknowledgement

This study was supported by a National Research Foundation of Korea (NRF) grant funded by the Korean government (MSIT) (No. 2017R1A5A1014883).

References

- [1] Z. Ma, J. Chung, P. Liu, H. Sohn, Bridge displacement estimation by fusing accelerometer and strain gauge measurements, Struct. Control. Health Monit. 28 (2021), e2733, <https://doi.org/10.1002/stc.2733>.
- [2] AASHTO, AASHTO LRFD Bridge Design Specifications, 8th edition, the American Association of State Highway and Transportation Officials, Washington, D.C., 2017. ISBN: 9781560516545.
- [3] MLTM, Korea highway bridge design code (in Korean), Ministry of Land, Infrastructure and Transport, Seoul, 2010. ISBN: 9788962951172.
- [4] MOHRD, GB 50017-2017 Code for Design of Steel Structures (in Chinese), China Machine Press, Beijing, 2020. ISBN: 9787111633167.
- [5] Z. Sun, D.M. Siringoringo, Y. Fujino, Load-carrying capacity evaluation of girder bridge using moving vehicle, Eng. Struct. 229 (2021), 111645, <https://doi.org/10.1016/j.engstruct.2020.111645>.
- [6] D. Hester, J. Brownjohn, M. Bocian, Y. Xu, Low cost bridge load test: calculating bridge displacement from acceleration for load assessment calculations, Eng. Struct. 143 (2017) 358–374, <https://doi.org/10.1016/j.engstruct.2017.04.021>.
- [7] D. Feng, M.Q. Feng, Identification of structural stiffness and excitation forces in time domain using noncontact vision-based displacement measurement, J. Sound Vib. 406 (2017) 15–28, <https://doi.org/10.1016/j.jsv.2017.06.008>.
- [8] S. Bhowmick, S. Nagarajaiah, Identification of full-field dynamic modes using continuous displacement response estimated from vibrating edge video, J. Sound Vib. 489 (2020), 115657, <https://doi.org/10.1016/j.jsv.2020.115657>.
- [9] D. Feng, M.Q. Feng, Model updating of railway bridge using in situ dynamic displacement measurement under trainloads, J. Bridg. Eng. 20 (2015) 04015019, [https://doi.org/10.1061/\(ASCE\)BE.1943-5592.0000765](https://doi.org/10.1061/(ASCE)BE.1943-5592.0000765).
- [10] K.V. Santhosh, B.K. Roy, Online implementation of an adaptive calibration technique for displacement measurement using LVDT, Appl. Soft Comput. 53 (2017) 19–26, <https://doi.org/10.1016/j.asoc.2016.12.032>.

- [11] S. Nakamura, GPS measurement of wind-induced suspension bridge girder displacements, *J. Struct. Eng.* 126 (2000) 1413–1419, [https://doi.org/10.1061/\(ASCE\)0733-9445\(2000\)126:12\(1413\)](https://doi.org/10.1061/(ASCE)0733-9445(2000)126:12(1413)).
- [12] H.H. Nassif, M. Gindy, J. Davis, Comparison of laser Doppler vibrometer with contact sensors for monitoring bridge deflection and vibration, *NDT & E Int.* 38 (2005) 213–218, <https://doi.org/10.1016/j.ndteint.2004.06.012>.
- [13] C. Gentile, G. Bernardini, Output-only modal identification of a reinforced concrete bridge from radar-based measurements, *NDT & E Int.* 41 (2008) 544–553, <https://doi.org/10.1016/j.ndteint.2008.04.005>.
- [14] G. Zhang, Y. Wu, W. Zhao, J. Zhang, Radar-based multipoint displacement measurements of a 1200-m-long suspension bridge, *ISPRS J. Photogramm. Remote Sens.* 167 (2020) 71–84, <https://doi.org/10.1016/j.isprsjprs.2020.06.017>.
- [15] L. Luo, M.Q. Feng, Edge-enhanced matching for gradient-based computer vision displacement measurement, *Comput. Aid. Civ. Infrastruct. Eng.* 33 (2018) 1019–1040, <https://doi.org/10.1111/mice.12415>.
- [16] I.-H. Chen, S.-C. Ho, M.-B. Su, Computer vision application programming for settlement monitoring in a drainage tunnel, *Autom. Constr.* 110 (2020), 103011, <https://doi.org/10.1016/j.autcon.2019.103011>.
- [17] Y. Narazaki, F. Gomez, V. Hoskere, M.D. Smith, B.F. Spencer, Efficient development of vision-based dense three-dimensional displacement measurement algorithms using physics-based graphics models, *Struct. Health Monit.* 20 (2021) 1841–1863, <https://doi.org/10.1177/1475921720939522>.
- [18] S. Yu, J. Zhang, Fast bridge deflection monitoring through an improved feature tracing algorithm, *Comput. Aid. Civ. Infrastruct. Eng.* 35 (2020) 292–302, <https://doi.org/10.1111/mice.12499>.
- [19] C.-Z. Dong, O. Celik, F.N. Catbas, Marker-free monitoring of the grandstand structures and modal identification using computer vision methods, *Struct. Health Monit.* 18 (2019) 1491–1509, <https://doi.org/10.1177/1475921718806895>.
- [20] H. Yoon, J. Shin, B.F. Spencer Jr., Structural displacement measurement using an unmanned aerial system, *Comput. Aid. Civ. Infrastruct. Eng.* 33 (2018) 183–192, <https://doi.org/10.1111/mice.12338>.
- [21] A. Havaran, M. Mahmoudi, Markers tracking and extracting structural vibration utilizing randomized Hough transform, *Autom. Constr.* 116 (2020), 103235, <https://doi.org/10.1016/j.autcon.2020.103235>.
- [22] J.-W. Park, D.-S. Moon, H. Yoon, F. Gomez, B.F. Spencer Jr., J.R. Kim, Visual-inertial displacement sensing using data fusion of vision-based displacement with acceleration, *Struct. Control. Health Monit.* 25 (2018), e2122, <https://doi.org/10.1002/stc.2122>.
- [23] Y. Xu, J.M. Brownjohn, F. Huseynov, Accurate deformation monitoring on bridge structures using a cost-effective sensing system combined with a camera and accelerometers: case study, *J. Bridg. Eng.* 24 (2019) 05018014, [https://doi.org/10.1061/\(ASCE\)BE.1943-5592.0001330](https://doi.org/10.1061/(ASCE)BE.1943-5592.0001330).
- [24] Z. Ma, J. Choi, H. Sohn, Real-time structural displacement estimation by fusing asynchronous acceleration and computer vision measurements, *Comput. Aid. Civ. Infrastruct. Eng.* 37 (2022) 688–703, <https://doi.org/10.1111/mice.12767>.
- [25] N. Wadhwa, M. Rubinstein, F. Durand, W.T. Freeman, Phase-based video motion processing, *ACM Trans. Graph.* 32 (2013) 1–10, <https://doi.org/10.1145/2461912.2461966>.
- [26] J.G. Chen, N. Wadhwa, Y.-J. Cha, F. Durand, W.T. Freeman, O. Buyukozturk, Modal identification of simple structures with high-speed video using motion magnification, *J. Sound Vib.* 345 (2015) 58–71, <https://doi.org/10.1016/j.jsv.2015.01.024>.
- [27] A. Sarrafi, Z. Mao, C. Niezrecki, P. Poozesh, Vibration-based damage detection in wind turbine blades using phase-based motion estimation and motion magnification, *J. Sound Vib.* 421 (2018) 300–318, <https://doi.org/10.1016/j.jsv.2018.01.050>.
- [28] Y.-J. Cha, J.G. Chen, O. Büyüköztürk, Output-only computer vision based damage detection using phase-based optical flow and unscented Kalman filters, *Eng. Struct.* 132 (2017) 300–313, <https://doi.org/10.1016/j.engstruct.2016.11.038>.
- [29] Z. Shang, Z. Shen, Multi-point vibration measurement and mode magnification of civil structures using video-based motion processing, *Autom. Constr.* 93 (2018) 231–240, <https://doi.org/10.1016/j.autcon.2018.05.025>.
- [30] J.G. Chen, A. Davis, N. Wadhwa, F. Durand, W.T. Freeman, O. Büyüköztürk, Video camera-based vibration measurement for civil infrastructure applications, *J. Infrastruct. Syst.* 23 (2017) B4016013, [https://doi.org/10.1061/\(ASCE\)IS.1943-555X.0000348](https://doi.org/10.1061/(ASCE)IS.1943-555X.0000348).
- [31] Z.Y. Wu, H.W. Shenton, D. Mo, M. Hmosze, Integrated video analysis framework for vision-based comparison study on structural displacement and tilt measurements, *J. Struct. Eng.* 147 (2021) 05021005, [https://doi.org/10.1061/\(ASCE\)ST.1943-541X.0003104](https://doi.org/10.1061/(ASCE)ST.1943-541X.0003104).
- [32] D.H. Diamond, P.S. Heyns, A.J. Oberholster, Accuracy evaluation of sub-pixel structural vibration measurements through optical flow analysis of a video sequence, *Measurement* 95 (2017) 166–172, <https://doi.org/10.1016/j.measurement.2016.10.021>.
- [33] L. Luan, J. Zheng, M.L. Wang, Y. Yang, P. Rizzo, H. Sun, Extracting full-field subpixel structural displacements from videos via deep learning, *J. Sound Vib.* (2021), 116142, <https://doi.org/10.1016/j.jsv.2021.116142>.
- [34] H. Bay, A. Ess, T. Tuytelaars, L. Van Gool, Speeded-up robust features (SURF), *Comput. Vis. Image Underst.* 110 (2008) 346–359, <https://doi.org/10.1016/j.cviu.2007.09.014>.
- [35] A. Smyth, M. Wu, Multi-rate Kalman filtering for the data fusion of displacement and acceleration response measurements in dynamic system monitoring, *Mech. Syst. Signal Process.* 21 (2007) 706–723, <https://doi.org/10.1016/j.ymssp.2006.03.005>.
- [36] K. Kim, J. Choi, J. Chung, G. Koo, I.-H. Bae, H. Sohn, Structural displacement estimation through multi-rate fusion of accelerometer and RTK-GPS displacement and velocity measurements, *Measurement* 130 (2018) 223–235, <https://doi.org/10.1016/j.measurement.2018.07.090>.
- [37] C. Shen, Y. Zhang, X. Guo, X. Chen, H. Cao, J. Tang, J. Li, J. Liu, Seamless GPS/inertial navigation system based on self-learning square-root cubature Kalman filter, *IEEE Trans. Ind. Electron.* 68 (2021) 499–508, <https://doi.org/10.1109/TIE.2020.2967671>.
- [38] C. Shen, Y. Xiong, D. Zhao, C. Wang, H. Cao, X. Song, J. Tang, J. Liu, Multi-rate strong tracking square-root cubature Kalman filter for MEMS-INS/GPS/polarization compass integrated navigation system, *Mech. Syst. Signal Process.* 163 (2022), 108146, <https://doi.org/10.1016/j.ymssp.2021.108146>.
- [39] S. Akhlaghi, N. Zhou, Z. Huang, Adaptive adjustment of noise covariance in Kalman filter for dynamic state estimation, in: 2017 IEEE Power & Energy Society General Meeting, IEEE, 2017, pp. 1–5, <https://doi.org/10.1109/PESGM.2017.8273755>.
- [40] Polytech GmbH, RSV-400 Scanning Vibrometer Datasheet. http://hysen.cafe24.co.m/wp-content/uploads/2019/10/OM_DS_PSV-400_2011_05_E.pdf, 2019 (accessed October 9, 2021).
- [41] Polytech GmbH, RSV-150 Scanning Vibrometer Datasheet. <https://www.atecorp.com/products/polytec/rsv-150>, 2019 (accessed March 24, 2022).